Pore Curvature Effect on the Stability of Co−MCM-41 and the Formation of Size-Controllable Subnanometer Co Clusters†

Sangyun Lim, Dragos Ciuparu, Yuan Chen, Yanhui Yang, Lisa Pfefferle, and Gary L. Haller*

Department of Chemical Engineering, Yale University, 9 Hillhouse Ave., New Haven, Connecticut 06520

Received: March 12, 2004; In Final Form: May 13, 2004

Samples of Co−MCM-41 with different pore diameters have been synthesized using organic templates with different alkyl chain lengths. The reducibility of cobalt in these highly stable samples was investigated by TPR and X-ray absorption spectroscopy. We have found that the reducibility correlates strongly with the pore diameter of the MCM-41, with the cobalt incorporated in the smaller pore MCM-41 being more resistant to complete reduction. It is proposed that the distribution of cobalt ions in the pore wall is affected by both the preparation procedure and the pore diameter. The size of the metallic Co clusters formed after different reducing treatments correlates linearly with the pore size, giving direct evidence for the effect of the radius of curvature on reducibility. Complete cobalt reduction after TPR causes an inverse variation of the cluster size with the pore size, resulting from differences in the density of Co clusters and from differences in the rate of Co migration and aggregation outside the pores of MCM-41 with different pore sizes.

Introduction

Patented by Mobil researchers in 1992,[1−6] the MCM-41 mesoporous molecular sieve structure has unique and intriguing scientific properties and potential practical applications. These materials have one-dimensional straight, cylindrical pores, which provide high surface area (> 1000 m^2/g). A wide range of pore diameters (2−10 nm) can be easily synthesized by changing the alkyl chain length of the template molecules and adding auxiliary organic molecules.[2,7−11] Because of the flexible structure of the amorphous silica wall, a number of metal components may be incorporated into the MCM-41 matrix without structural collapse. The chemical composition and pore size of MCM-41 can be varied independently, providing a material for the systematic investigation of the dependence of the catalytic and physical properties on the pore radius of curvature. MCM-41 materials have been studied as model catalysts for shape-selective reactions of large molecules,[12,13] as a catalytic membrane,[14,15] and for other reactions such as reforming,[16] oxidation,[17−20] photosynthesis,[21] polymerization,[22−26] etc. Its simple, regular, and controllable pore structure makes MCM-41 materials suitable also for the systematic investigation of the adsorption characteristics[27−29] aiming to develop adsorption models for mesoporous molecular sieve materials.[30−32] Recently, a preliminary study of Co−MCM-41 as an effective catalyst for the growth of single-walled carbon nanotubes has been reported.[33,34]

The low hydrothermal and mechanical stability of the metal-substituted MCM-41 materials has been a major drawback in using them as catalysts. By modifying the original synthesis conditions, that is, mixing effect, pH, antifoam agent, silica source, autoclaving temperature and time, etc., some of these physical problems have been more or less solved.[35,36] However, the distribution of isomorphously substituted metal components in MCM-41, which may substantially affect the catalytic activity and stability, has not yet been reported. We have previously noted that Co−MCM-41 is quite stable against redox cycles at high temperatures (1173 K)[34] under oxidation conditions due to the formation of cobalt orthosilicate on the surface at 1123 K.[37]

Several previous studies have discussed the dependence of the Co metal cluster size on the pore size of MCM-41.[38−41] In these studies, however, the Co−MCM-41 catalyst was prepared by impregnation of the siliceous MCM-41 and the size of the Co particles resulting from the reduction of these catalysts were in the range of a few nanometers. It should be noted that the reduction temperature and, thus, the temperature at which a metal cluster forms, was relatively low (573−673 K). It is therefore expected that, without any confinement or anchoring, further aggregation resulting in larger size particles will take place during exposure of these catalysts to the higher temperatures often required for catalytic applications.

In an attempt to prevent cobalt sintering, we incorporated the metal component in the MCM-41 framework with quasi-atomic scale dispersion. We have shown that this procedure allows the stabilization of ultrasmall metal clusters. Here we use temperature programmed reduction (TPR) and X-ray absorption (XANES and EXAFS) to investigate the stability of the Co-incorporated MCM-41 with different pore sizes under a variety of reducing conditions. We focus on the effect of the radius of curvature of the pore on the size of the Co metal cluster formed from Co−MCM-41 with five different average pore diameters ranging from 1.8 to 3.1 nm, as measured by the BJH method.[42]

Experimental Section

Preparation of Co−MCM-41 Samples. C10−C18 Co−MCM-41 samples were synthesized by a modified Beck[1−6] method, as described elsewhere.[34] Fumed silica (Cab-O-Sil, Cabot Corporation), tetramethylammonium silicate (16.9% TMASi, Aldrich), deionized water, and cobalt sulfate (Aldrich) aqueous solution were mixed for 30 min. The water to total silica mol ratio was set at 86 for all samples. The surfactant solutions (C10−C18) were added to the prepared silica and Co

† Part of the special issue "Michel Boudart Festschrift".

* To whom correspondence should be addressed.

10.1021/jp048881+ CCC: $30.25
Published on Web 07/02/2004

mixture, and a small amount of antifoaming agent (0.2 wt % of surfactant) was incorporated to remove excess foam produced by the surfactant as a result of vigorous stirring of the synthesis solution. Acetic acid (Baker) was added until pH = 11.5 was reached. After additional mixing for about 30 min, this synthesis solution was poured into a polypropylene bottle and placed in an autoclave at 373 K for 6 days. After cooling to room temperature, the resulting solid was recovered by repeated filtration and washing with deionized water, and dried under ambient conditions overnight. The predried solid was then heated from room temperature to 813 K for 20 h under ultrahigh purity He (30 mL/min) and soaked for 1 h at 813 K in flowing He followed by calcination for 6 h at 813 K under flowing ultrazero grade air to remove residual organics. The molar ratio of each component in the synthesis solution was fixed at a SiO_2: surfactant:Co:H_2O molar ratio of 1:0.27:0.01:86. Because the preparation process may cause some loss of Co and silica in the byproducts, the final Co content of each sample was determined by ICP at Galbraith Lab., Inc. The physicochemical properties of the prepared Co−MCM-41 samples were characterized by XRD, nitrogen physisorption, UV−vis, X-ray absorption, and TEM, and the results are given and discussed in detail elsewhere.[34]

Temperature Programmed Reduction (TPR). The reducibility and the stability of C10−C18 Co−MCM-41 samples prepared were investigated by a temperature programmed reduction technique using the thermal conductivity detector (TCD) of gas chromatography (6890 plus, Agilent). Approximately 200 mg of each sample was loaded into a quartz cell. Prior to each TPR run, the sample cell was purged by ultrazero grade air at room temperature, then the temperature was increased to 773 K at 5 K/min, soaked for 1 h at the same temperature, and cooled to room temperature. This procedure produces a clean surface before running the TPR. The gas flow was switched to 5% hydrogen in argon balance, and the baseline was monitored until stable. After baseline stabilization, the sample cell was heated at 5 K/min and held for 1 h at 1173 K to ensure complete cobalt reduction. An acetone trap was installed between the sample cell and the TCD to condense water, produced by sample reduction.

X-ray Absorption (XANES and EXAFS). As a complementary experiment to TPR and for the measurement of Co cluster size, in situ and ex situ X-ray absorption measurements were performed at the Co K edge (7709 eV) using Si (111) as the monochromator crystal at station X23A2 in NSLS, 2.5 GeV storage ring, Brookhaven National Laboratory. Eighty mg of each sample was pressed into a self-supporting wafer and placed in a stainless steel cell equipped with beryllium (0.5 mm thick, Aldrich) windows, gas inlet and outlet, liquid nitrogen cooling line, and heating elements allowing in situ controlled atmosphere treatments up to 1023 K. To characterize the effect of the reduction temperature, each sample was reduced at 773 K and 973 K by flowing ultrahigh purity hydrogen for 30 min to 1 h and quenched at 273 K using the liquid nitrogen cooling line. X-ray absorption near edge structure (XANES) spectra were collected during sample reduction with a 5 min interval between scans. Extended X-ray absorption fine structure (EXAFS) spectra were also recorded for the measurement of Co cluster sizes of samples after each sample treatment described above. Because the samples were exposed to air after TPR, a mild reduction at 673 K for 30 min was carried out to reduce the partially oxidized Co prior to recording the EXAFS spectra. The spectra collected were analyzed using the UWXAFS analysis package.[43]

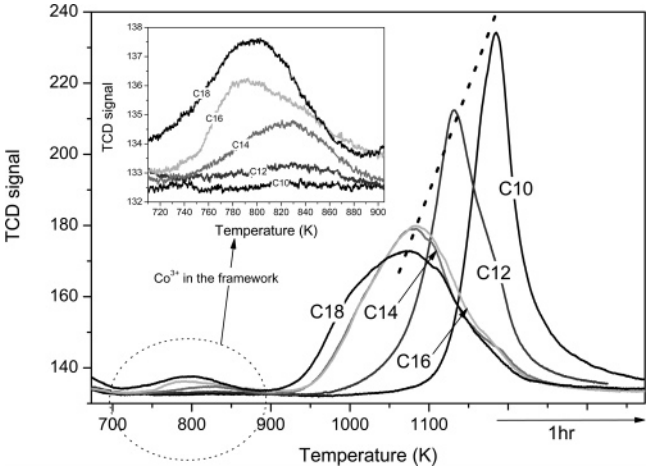

Figure 1. Temperature programmed reduction (TPR) results of Co−MCM-41 samples.

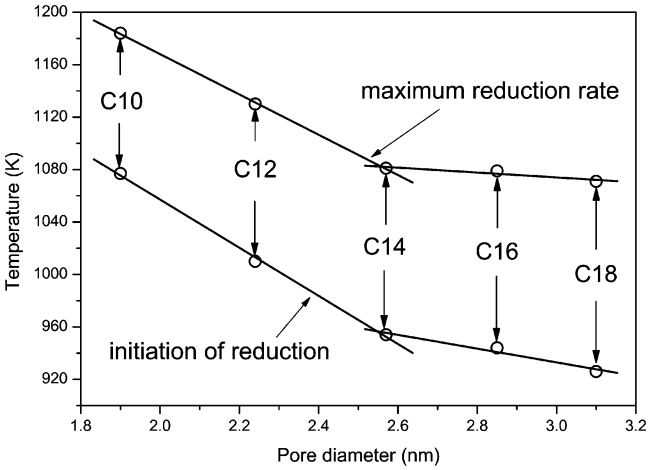

Figure 2. Changes of reduction temperature of Co−MCM-41 samples with pore diameters.

Results and Discussion

Temperature Programmed Reduction (TPR). TPR is a useful characterization technique for investigating and designing a catalyst. It can provide important surface chemical information such as material species, stability, metal distribution, etc. In this study, TPR was carried out in the temperature range from 323 K to 1173 K for the purpose of investigating the reduction temperature of the cobalt species in Co−MCM-41 as a stability index.

The TPR profiles for samples having the same cobalt loading but different pore diameters are shown in Figure 1. Co−MCM-41 samples having different pore diameters show different reduction patterns. There were no reduction peaks under 673 K, where surface cobalt oxides were previously observed to reduce in our test runs with Co_3O_4 and CoO, suggesting that Co was entirely incorporated into the silica framework, as discussed elsewhere.[34] In addition, there is a systematic change in the temperature at the maximum reduction rate (summit of the peak) and in the temperature of reduction initiation. Both of these temperatures increase monotonically with increasing pore size. These two temperatures are plotted for clarity against the pore diameter in Figure 2. A mechanism that might explain this observation is the change in silica structure at high radius of curvature proposed by Feuston et al.[44] This group suggested that by reducing the micelle size of the template and thus, the pore diameter of the resulting MCM-41 material, the curvature

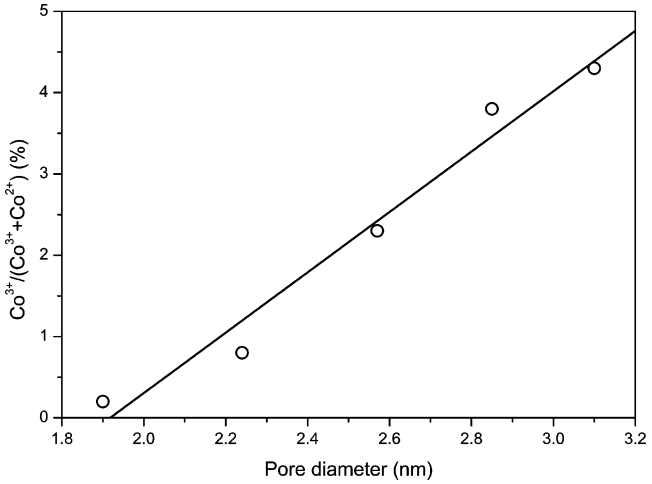

Figure 3. Quantification of Co^{3+} with pore diameters of Co−MCM-41 samples.

of the oxygen-terminated silica surface is increased, causing the distribution of silica rings to shift to smaller ring sizes. Galeener[45] demonstrated this shift using both calculations and polarized Raman spectroscopy to measure the distribution of silica ring sizes and explained that the small silica rings become larger by unpuckering. The ring structure can only relax by breaking a bond and incorporating itself into a ring of larger order. Along these lines, it is proposed that in the Co−MCM-41, where some of the Si atoms are substituted by Co atoms, the smaller ring structure in small pores is more difficult to break than larger rings in large pores, thus resulting in a higher reduction temperature for cobalt incorporated in smaller pore diameter MCM-41.

In addition to the main TPR feature there is a lower reduction peak around 800 K that is tentatively attributed to Co^{3+} in the silica framework. These species may have been formed during Co−MCM-41 calcination,[34] and their amount increases with the pore size of the Co−MCM-41. Thus, assigning the first reduction peak to Co^{3+} and the second one to Co^{2+}, the fraction of Co^{3+} in each Co−MCM-41 sample was determined from the peak area calculations and plotted against the pore size in Figure 3. The Co^{3+} content is less than 5% in all Co−MCM-41 samples, and increases with the pore size of Co−MCM-41.

Another interesting feature observed in the TPR profiles in Figure 1 are the differences observed in the shape (heights and widths) of the reduction peaks for Co−MCM-41 of different pore sizes. The peak height decreases linearly from C10 to C18 Co−MCM-41. Since, regardless of the pore size, all the Co−MCM-41 samples have 1 wt % Co loading, the concentration of the Co atoms per unit volume of solid Co−MCM-41 increases when the pore diameter decreases, assuming the same wall thickness and Co/Si ratio. This is simply a consequence of the overall material density, which increases when the pore diameter decreases because the pore volume decreases. Assuming the Co reduction kinetics to be of positive order with respect to the Co ion concentration, an increase of the concentration of Co should result in a higher reduction rate and result in a narrower reduction peak in the TPR. However, the dominant effect is simply that when the reduction is initiated at a higher temperature, the rate is higher and the peak is narrower. The peak areas and the full width at half-maxima (fwhm) were determined for the reduction peaks of the Co^{2+} species for each Co−MCM-41 sample. As expected for samples having the same cobalt loading, there are no significant changes in the peak areas, while the fwhm increases linearly with the pore size of Co−MCM-41 indicating slower cobalt reduction kinetics for larger pore diameters.

Intuitively, there may also be an effect of the location of the Co ions in the MCM-41, that is, at the pore wall surface, near the pore wall surface or in the "bulk" of the 1 nm thick pore walls. Cobalt near the pore wall surface is expected to be easier to reduce than that located in the bulk, resulting in a higher rate of reduction. Assuming a constant pore wall thickness of 1 nm,[34] and a calculated Co^{2+} ionic radius of 0.072 nm,[46] when Co is incorporated and dispersed at the atomic scale in the silica framework there may be several layers of Co in the pore wall, such as just at the surface, in the center of the wall, and between these locations. Taking into account the location of cobalt ions in the MCM-41 pore walls, the slight asymmetry of the Co^{2+} reduction peak of the TPR profiles can be decomposed into three Co^{2+} reduction peaks by deconvolution. A deconvolution of the TPR profile was performed for each Co−MCM-41 sample with different pore size, and each integrated peak area (assigned as peak 1, 2, and 3) is plotted against the pore size in Figure 4. Peaks 1 and 2 were assumed to be Co ions distributed near the pore wall surface, which can be reduced more easily than Co ions in the middle of the pore walls (bulk silica, peak 3). The amount of surface Co ions increases as the pore size of the Co−MCM-41 decreases, resulting in less Co buried in the silica bulk. The reduction rate of the surface Co should be much faster than those in the bulk, resulting in narrower and taller reduction peaks. However, C18 Co−MCM-41 showed a dramatically reduced amount of Co in the bulk (most of the Co ions are distributed near the surface), probably due to the low purity of C18 surfactant (octadecyltrymethylammonium bromide), as noted with less-pure silica source (HiSil 915).

We note that this interpretation is not unique. An alternative hypothesis might be that reducibility is associated with the degree of hydroxylation of the nearest Si, for example, ═Si$(OH)_2$, ═SiOH, and ═Si═, but this would have to assume all Co was "in" the surface. (This hypothesis could be checked by simultaneously measuring the degree of hydroxylation by IR and/or ^{29}Si NMR.) More complicated models are also possible, and it is probable that there are contributions from local silica cycle size/structure, Co proximity to the surface, and Co proximity to surface hydroxyls. The important observation is that the reducibility correlates with pore size and is probably associated with Co distribution/structure with respect to the pore wall surface.

The Co−MCM-41 showed a remarkable physical and structural stability against thermal and mechanical stress.[34] This was the case for the Co−MCM-41 where the Co was still in the framework or partially reduced. After TPR, all Co atoms are reduced and converted to Co metal clusters, which are completely removed from the silica framework and may cause the MCM-41 structure to collapse. Nitrogen physisorption was performed for a C16 Co−MCM-41 sample recovered after TPR and compared in Figure 5 with the one recorded for the fresh sample. Surprisingly, there is little difference between the physical structures of the fresh and after-TPR samples. The surface area, pore volume, and the fwhm of pore size distribution are virtually identical for the two samples. The slopes of the capillary condensation (a measure of structural order[47]) and the pore size are slightly decreased after TPR, which may be attributed to a thermal contraction and to the presence of Co metal clusters on the surface of the pore walls. The inset TEM picture in Figure 5 (b) was recorded for a C16 Co−MCM-41 sample after TPR. The pore entrances and long range order of

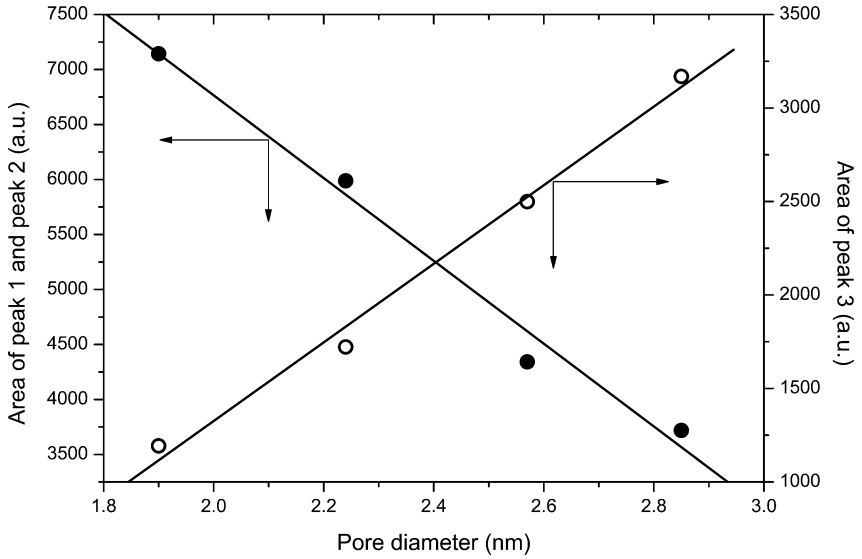

Figure 4. Area of deconvoluted reduction peak with pore diameter of Co−MCM-41 samples.

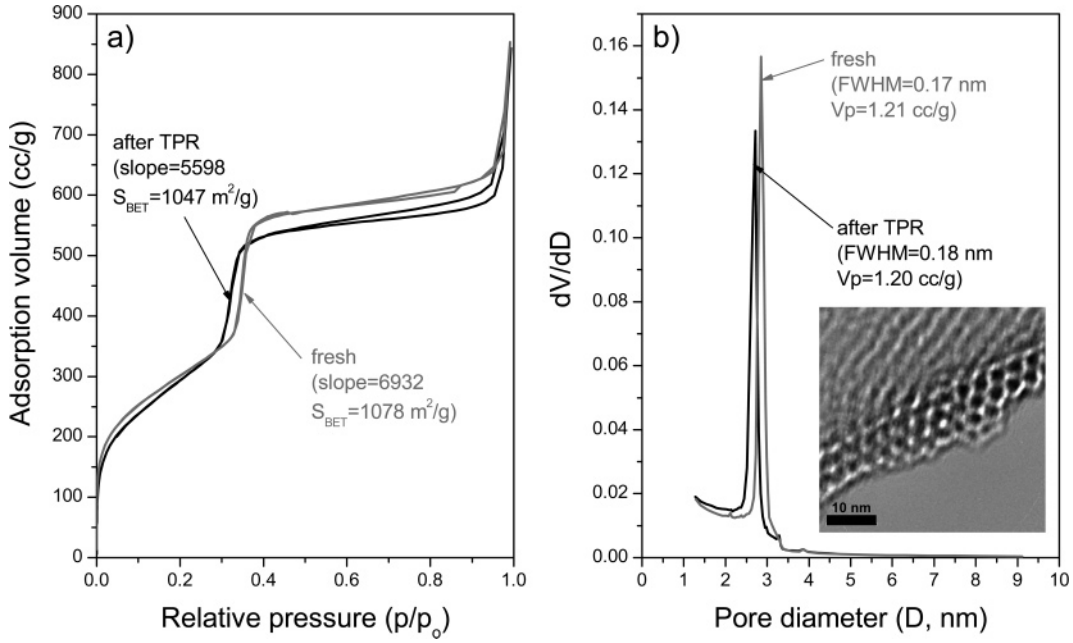

Figure 5. Nitrogen physisorption results between fresh and after TPR C16 Co−MCM-41 samples; isotherms b) pore size distributions (inset: TEM picture of C16 Co−MCM-41 after TPR).

the pore walls are clearly observed in this micrograph. This gives direct evidence that the Co−MCM-41 prepared in this study using a high purity silica source (Cab-O-Sil, 99.8% SiO_2) and accurate pH adjustment to 11.5 has an extremely stable physical structure and maintains order after Co removal from the framework by a harsh thermal reduction at 1173 K for 1 h under flowing hydrogen.

X-ray Absorption Spectroscopy (XANES and EXAFS). The TPR experiments above gave evidence of a linear correlation between the pore radius of curvature and the Co reduction temperatures. It is of interest, for many potential applications in catalysis, to determine if the size of the cobalt clusters formed in the MCM-41 silica matrix is also influenced by the pore radius of curvature. We have previously shown that cobalt clusters of different sizes were obtained during synthesis of single-wall carbon nanotubes in Co−MCM-41 catalysts of different pore diameters.[33] It is, therefore, expected that the size of cobalt clusters obtained by reduction of the cobalt incorporated by isomorphous substitution of Si in the MCM-41 framework would correlate with the pore size of MCM-41. We will furthermore contemplate the prospect of controlling the size of these clusters by using specific reduction conditions for Co−MCM-41 of different pore radiuses of curvature. The X-ray absorption spectroscopy was employed to characterize the changes in the local coordination of the Co in the Co−MCM-41 samples with different pore sizes at different stages in the reduction process. The size of the cobalt clusters was determined from the EXAFS spectra considering the average first shell Co−Co coordination number for each sample.

The XANES spectra recorded for fresh C10−C18 Co−MCM-41 samples dehydrated at 773 K for 30 min under flowing air (not shown) are superimposable. The pre-edge peak is similar to that observed for $CoAl_2O_4$, confirming the tetrahedral coordination of the cobalt ions surrounded by oxygen anions in the pore walls.[34] The average first shell Co−O coordination numbers vary from 4.0 to 4.7 (see Table 1), suggesting the Co ions are incorporated by isomorphous substitution of Si in the silica framework without formation of any surface cobalt oxide

TABLE 1: The Average First Shell Co−O Coordination Numbers of Hydrated and Dehydrated Co−MCM-41 Samples

	Co-O coordination number		
samples	dehydrated	hydrated	Δ in hydration
C10 Co−MCM-41	4.67	5.48	0.81
C12 Co−MCM-41	4.63	5.65	1.02
C14 Co−MCM-41	4.52	5.78	1.26
C16 Co−MCM-41	4.49	5.78	1.29
C18 Co−MCM-41	4.04	5.19	1.15

compounds. We should note here that the average Co−O coordination number systematically increases from 4.0 to 4.7 as the pore size decreases. However, this apparent increase in coordination number may only reflect a change in transition probability that is caused by changes in bond angle when Co is incorporated into smaller ring structures in smaller pores of greater radius of curvature. Note also that the difference between the hydrated and dehydrated states decreases with pore size, particularly between C14, C12, and C10, which exhibit the larger change in reducibility (see Figure 2). This increase in hydrophobicity and apparent Co−O coordination with decreased pore size is consistent with a distribution toward more Co in the wall small rings, relative to the wall larger silica rings, with decreasing pore size.

We have previously defined the Co state in Co−MCM-41 as a mixture of tetrahedral and distorted tetrahedral coordination of Co^{2+} and Co^{3+}, respectively, with a pseudo-octahedral environment attained at some sites due to hydration.[34] Along these lines, there may be some differences in the Co−O coordination number between hydrated and dehydrated samples because one is tetrahedral and the other is of pseudo-octahedral structure. A hydrated sample was prepared by exposing the Co−MCM-41 overnight to the ambient atmosphere. The color changed from light blue to grayish blue, suggesting the Co local coordination has changed. The XANES spectra of hydrated and dehydrated Co−MCM-41 samples did not show any differences in the pre-edge peaks (associated primarily with Co ion symmetry), but the white line decreases after dehydration. The decrease in white line intensity is not expected if dehydration simply removes coordinated water molecules from the Co ions (which should increase the density of empty states on Co and thus increase white line intensity). Perhaps dehydration is primarily the result of dehydroxylation of Si coordinated to Co and the increased average charge on Si is inductively transferred to Co. This observation is not completely understood.

The average first-shell Co−O coordination numbers between two conditions are listed in Table 1. All dehydrated samples show coordination numbers between 4.04 and 4.67, confirming again that the Co atoms have approximate tetrahedral coordination with the surrounding oxygen anions and have successfully substituted Si atoms in the framework. The hydrated samples, however, show higher coordination numbers (5.19−5.78) than dehydrated samples. This finding is also consistent with the proposed explanation for the increased coordination number for smaller pore diameters discussed above and may be attributed to the water molecules contacting directly the Co centers to make pseudo-octahedral species. However, one would not expect the Co−O bond length of oxide ions and oxygen of coordinated water to be the same. A two shell fit does improve the fit and the second shell (of coordinated water) is very long (∼ 0.35 nm) and too large to be realistic physically. Note that this suggests that a significant fraction of the Co ions must be exposed in the pore wall surface. These numbers between

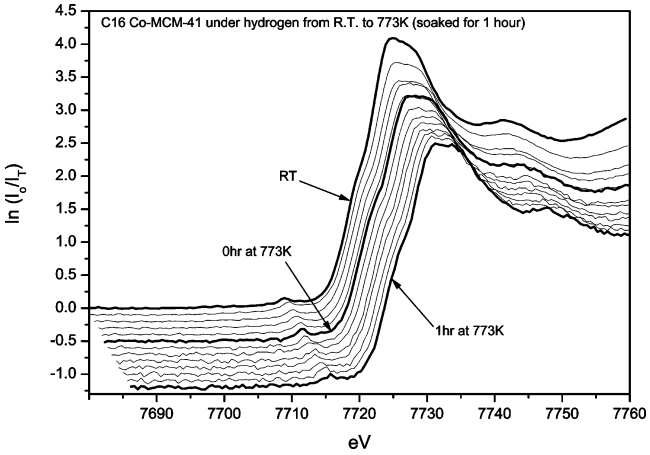

Figure 6. Temperature-programmed reduction of C16 Co−MCM-41 measured by XANES from room temperature to 773 K.

hydrated and dehydrated samples are reversible. The same phenomenon was previously observed in V−MCM-41.[48]

The lowest reduction initiation temperature observed in our TPR experiments was higher than 900 K (C18 Co−MCM-41) under a 5% H_2/Ar atmosphere. Using pure hydrogen, however, the reduction temperature would be expected to be lower. An in situ XANES TPR was performed using ultrahigh purity hydrogen from room temperature to 773 K at 20 K/min, continuously monitoring the state of the Co in Co−MCM-41. Surprisingly, at this condition there is no significant difference in any of the 5 different diameter samples run. The XANES spectra recorded during the TPR experiment performed with the C16 Co−MCM-41 sample are given as an example in Figure 6. The Co pre-edge spectral feature does not change even after 1 h at 773 K, consistent with our previous results on Co−MCM-41.[34] The only change observed is a decrease in the intensity of the white line suggesting some loss of oxygen by reduction. This behavior is again direct evidence for the remarkable stability of Co−MCM-41.

A similar experiment performed at a higher temperature (973 K) and depicted in Figure 7 (only for C10 and C16 Co−MCM-41 samples) shows that each sample has its own, specific reduction pattern. As in the earlier TPR experiments, the degree of reduction was observed to increase as the pore size increases. While the C16 Co−MCM-41 sample started to form metallic Co clusters after 6 min at 973 K, the C10 Co−MCM-41 does not show clear Co metal spectral features after being submitted to the same severe reduction conditions. Formation of a Co metal phase is evidenced by the sudden decrease of the white line intensity for each sample associated with the appearance of the characteristic pre-edge feature of the metal. It was concluded from this result that Co metal clusters may have been formed on the pore wall surface after reduction at 973 K for 30 min, and their sizes are affected by the pore radius of curvature, as was the case for samples after TPR.

The EXAFS spectra were recorded at room temperature after each of the XANES TPR experiments performed with Co−MCM-41 samples of different diameters and were used to determine the average first shell Co−Co coordination numbers. The EXAFS data fitting followed a procedure described elsewhere[49] using a rectangular window for k and R spaces with k weight equal1.

Carbon monoxide disproportionation was used as another method of control of Co cluster size. When the Co−MCM-41 is completely reduced with hydrogen, the metallic clusters formed can move freely at the surface to nucleate larger

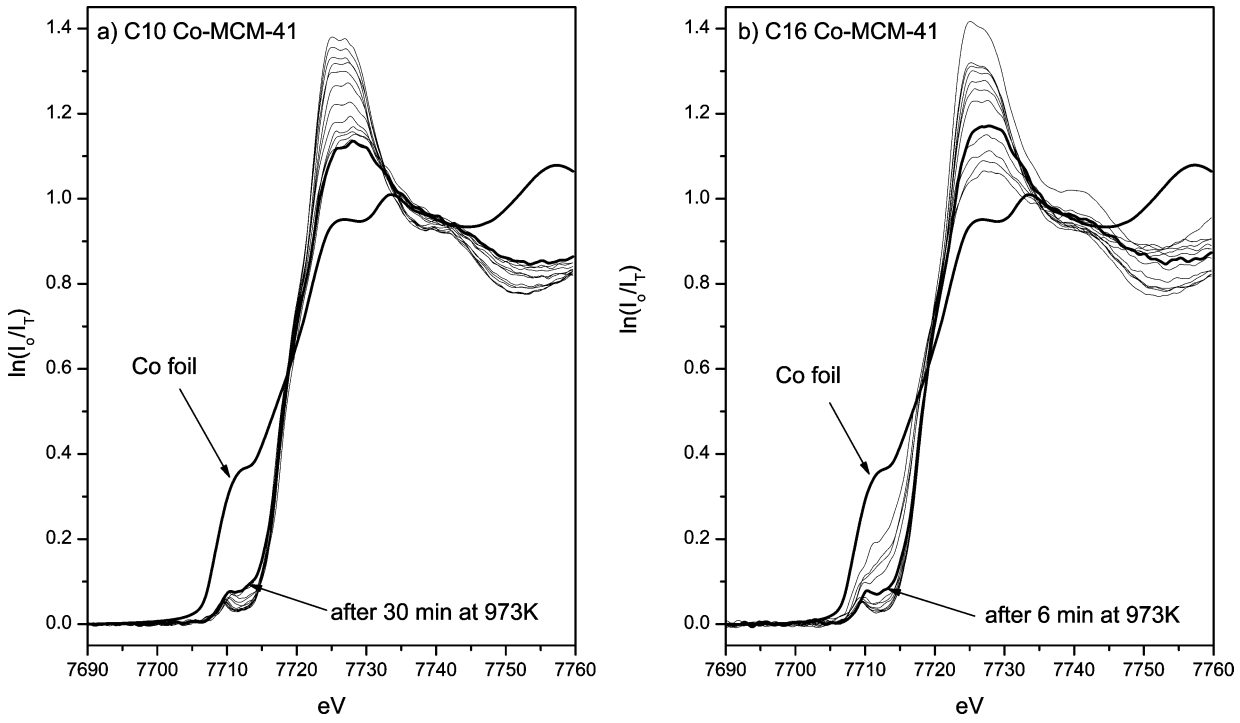

Figure 7. Temperature-programmed reduction of C10 and C16 Co−MCM-41 samples measured by XANES from room temperature to 973 K.

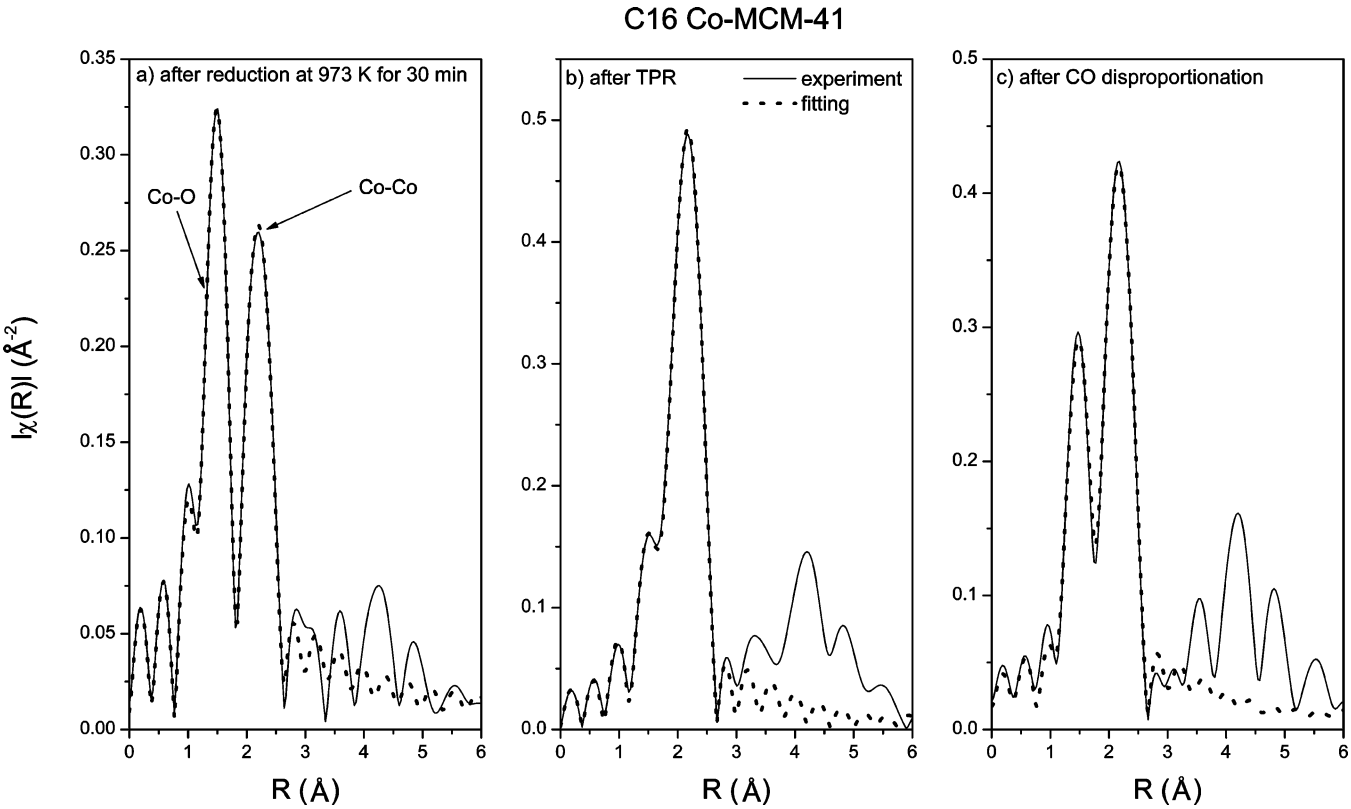

Figure 8. R space fitting results of C16 Co−MCM-41 treated by different conditions.

particles. By contrast, the metallic clusters formed during synthesis of carbon nanotubes by CO disproportionation become covered with carbon as soon as they initiate the growth of a carbon nanotube or other type of carbon at their surface, thus becoming immobilized and unable to sinter. Therefore, the rate of Co cluster growth will be constrained by the carbon deposited at their surface. While the carbon nanotube growth procedure is described in detail elsewhere,[33] a typical R space fitting of the EXAFS spectra recorded for a C16 Co−MCM-41 sample after carbon deposition by CO disproportionation is given as an example in Figure 8 along with those obtained for the same catalysts submitted to TPR or reduced at 973 K for 30 min. Because small metallic cobalt clusters are rapidly oxidized by exposure to ambient atmosphere, the sample after TPR was reduced at 673 K for 30 min prior to in situ recording of the X-ray absorption spectra. We expect to completely recover the clusters formed during TPR without affecting their size. However, if there is any incomplete reduction, the oxide left

TABLE 2: Degree of Reduction of Co−MCM-41 Samples Calculated from the Pre-edge Peak Area of XANES Spectra

experiment condition	samples	area of Co peak by gaussian fitting (%)
in situ	C16 Co−MCM-41 after TPR	0.38 (100)[1]
	C10 Co−MCM-41 after reduction at 973K for 30min	Trace
	C12 Co−MCM-41 after reduction at 973K for 30min	Trace
in situ	C14 Co−MCM-41 after reduction at 973K for 30min	0.09 (23.7)
	C16 Co−MCM-41 after reduction at 973K for 30min	0.12 (31.6)
	C18 Co−MCM-41 after reduction at 973K for 30min	0.21 (55.3)
	C10 Co−MCM-41 after CO disproportionation[2]	0.22 (57.9)
	C12 Co−MCM-41 after CO disproportionation[2]	0.24 (63.2)
ex situ	C14 Co−MCM-41 after CO disproportionation[2]	0.27 (71.1)
	C16 Co−MCM-41 after CO disproportionation[2]	0.29 (76.3)
	C18 Co−MCM-41 after CO disproportionation[2]	0.36 (94.7)

[1] 1.36×10^{-5} mole (1 wt % Co of 80 mg Co−MCM-41) [2] prereduced at 773 K for 30 min with pure hydrogen

TABLE 3: The First Shell Average Co−Co and Co−O Coordination Numbers of Co−MCM-41 Samples Treated in Various Ways

	first shell average coordination number					
	after reduction at 973 K for 30 min		after CO disproportionation at 1073 K for 1 hour		after temperature programmed reduction (TPR)	
pore diameter (nm)	Co−Co	Co−O	Co−Co	Co−O	Co−Co	Co−O
1.90 (C10)*	1.15	3.35	6.13	2.03	9.90	0.55
2.24 (C12)*	2.97	2.76	6.56	2.01	9.37	0.59
2.57 (C14)*	4.65	1.81	6.98	1.54	8.47	0.56
2.85 (C16)*	4.86	1.73	7.17	1.36	8.04	0.55
3.10 (C18)*	6.31	1.24	7.43	0.70	7.52	0.61

()*: carbon number of surfactant

should be in octahedral coordination, thus different than the cobalt incorporated in the silica framework. The fittings were very good for all cases. After CO disproportionation, there are slight differences in the nodes of Co−O compared to other samples. A possible compound after CO disproportionation is cobalt carbide (Co_2C or Co_3C). In this case, Co−C is almost identical to Co−O; therefore, this subtle difference may be from the interference between Co−O and Co−C caused by carbons covering the surface of the Co−clusters. The sample after TPR shows mainly metallic Co with a small Co−O residue. Some cobalt metal clusters may have been oxidized immediately by exposure to the ambient atmosphere. Cobalt was reduced again at 673 K for 30 min before the in situ X-ray absorption experiment to reconstitute the Co metal. However, this may not be sufficient to reduce all oxidized Co clusters.

To quantify the reduction state of Co atoms, the degree of reduction of Co-substituted MCM-41 samples was calculated from the Co pre-edge peak area of XANES spectra of each sample for different treatment conditions. The C16 Co−MCM-41 sample after TPR was used to normalize the degree of reduction of each sample. The area of the pre-edge peak observed in the spectra of the C16 Co−MCM-41 sample with 1 wt % Co after TPR was considered as a reference for 100% reduction because all the Co atoms in this sample were completely reduced. The pre-edge peak areas of the other samples were divided by this value, and the results are shown in Table 2. The degree of reduction of Co atoms increases with the pore diameter of Co−MCM-41 samples, as would be predicted. Over half of the Co atoms are still oxidized in the framework after reduction by pure hydrogen at 973 K for 30 min. The C10 and C12 Co−MCM-41 samples are essentially unreduced even after this severe reduction condition. After CO disproportionation at 1073 K for 1 h, however, more Co atoms are reduced; 95% of the Co atoms are reduced in the C18 Co−MCM-41 sample. These samples still show a high degree of reduction from 58% to 95%, although the XANES spectra were collected under ex situ conditions. This suggests that there is a serious oxygen diffusion resistance through the carbon layers formed on the surface of the Co clusters, resulting in a barrier to continued growth of the metal clusters. The pore radius of curvature effect on the degree of reduction of Co-MCM-41 samples is clearly shown.

The average first shell coordination numbers of Co−Co and Co−O in Co−MCM-41 samples with different pore sizes are shown in Table 3. As expected, the Co−Co coordination number of samples reduced by hydrogen at 973 K increases as the pore size increases and the Co−O coordination number decreases. The Co−Co coordination numbers for the sample after CO disproportionation are larger than those of the sample reduced at 973 K. This behavior is expected since the reduction at 973 K is less severe than the reduction conditions during CO disproportionation for 1 h at 1023 K following the prereduction at 773 K for 30 min by hydrogen. It should also be noted that the Co−Co coordination numbers in the catalysts after carbon deposition change less with the pore size than in the case of the samples reduced at 973 K. This behavior is also consistent with the carbon layer impeding cluster nucleation, and suggests that there is a certain size of the Co clusters required for CO dissociation and growth of carbon on the surface.

However, the samples after TPR show an opposite trend, that is, the Co−Co coordination numbers are larger for the cobalt clusters formed in Co−MCM-41 with smaller pores. After TPR, all Co atoms are completely reduced and removed from the bulk silica pore wall, resulting in free mobility on the surface and, thus, no confinement by the pore walls. This, therefore, might be attributed to the more rapid migration of smaller Co clusters initially formed in the small pores, which then form larger Co clusters outside the pores without confinement by the pore walls. After CO disproportionation, the Co−Co coordination numbers are between the other two cases. This may be due to reduction in two stages, by hydrogen and CO. Samples were prereduced by hydrogen at 773 K for 30 min, and the CO disproportionation was performed at 1073 K for 1 h. After prereduction by hydrogen, the Co clusters continue to grow under CO, and the

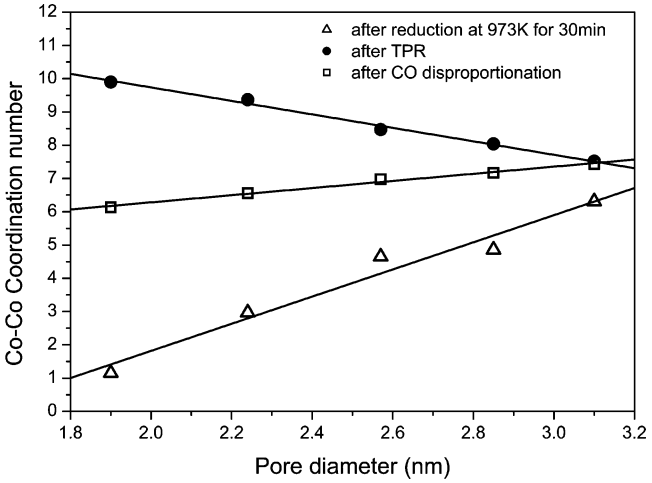

Figure 9. Changes of average first shell Co−Co coordination numbers with pore diameters.

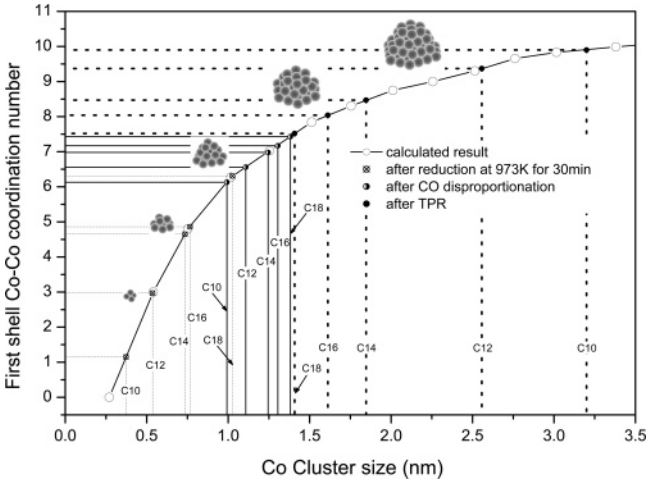

Figure 10. Average first shell Co−Co coordination number vs cluster diameter created by the cobalt (111)-truncated hemispherical cuboctahedron model.

growth may stop at a certain point due to carbonization of the Co cluster surfaces, resulting in diffusion-limited reduction to metal particles and/or inhibited metal sintering. It is noteworthy that the increase of the Co−Co coordination number with increasing pore size of Co−MCM-41 samples after CO disproportionation is less significant than after reduction by hydrogen at 973 K for 30 min. Prereduction by hydrogen followed by CO contact further reduces the Co atoms, and the Co cluster keeps growing until carbon starts to deposit on the surface to confine further growth. This suggests that there is a Co cluster critical size required to deposit carbon on the surface. Alternatively, we may assume that dissociative chemisorption of CO is a function of Co cluster size. The Co−Co coordination numbers for Co−MCM-41 samples of different pore sizes following different treatment conditions are illustrated in Figure 9. Reduction by hydrogen, or by hydrogen followed by CO, results in increased Co cluster size with pore size. Reduction by hydrogen only at very high temperature (after TPR) results in an inverse correlation, presumably because Co cluster size is dominated by the kinetics of migration out of the pores under these conditions as opposed to the kinetics of reduction and nucleation in the pores for the other two cases.

We hypothesize that one mechanism of stabilizing the very small Co clusters in pores of MCM-41 may be bonding between the metal cluster and Co ions bonded to the silica matrix. A similar effect has been observed for Rh and Pt metal clusters anchored to Cr^{3+} and Fe^{2+} ions in Y-zeolite, which improves the stability and dispersion of Rh and Pt.[50,51] That is, small Co clusters formed by hydrogen-only reduction at 973 K for 30 min and CO disproportionation may still be bonded to unreduced Co atoms in the framework, which have an effect through the pore wall radius of curvature on its sizes. The degree of reduction of small pore Co−MCM-41 is lower than large pore, which suggests that there are more chances for small metal clusters to anchor on ions on the pore wall surface. Before complete reduction, therefore, Co cluster sizes are confined by the pore radius of curvature, resulting in smaller cluster size in the small pores. There, however, can be no physical constraint by the pore walls after finishing TPR because most of the cobalt has migrated out of the pores and there is no possibility of anchoring of Co clusters to Co ions in the walls due to the complete reduction of Co.

For particles with diameters smaller than 3−5 nm, the coordination number is a strong and nonlinear function of the particle diameter.[49] This property has been widely used in EXAFS analysis to determine the size of nanoparticles.[52,53] The Co−Co first shell coordination numbers obtained from the EXAFS spectra were used to determine the approximate size of the cobalt clusters formed during each treatment. A (111)-truncated hemispherical cuboctahedron model was built to correlate the cobalt clusters diameter with the average first shell coordination number as shown in Figure 10. The samples reduced by hydrogen at 973 K for 30 min show the Co cluster size under 1 nm for all pore sizes. After CO disproportionation, all Co clusters are in the range of 1−1.5 nm, which is the narrowest window of cluster size distribution among three treatments in this study. After TPR, the sequence of cluster sizes, with respect to MCM-41 pore size, is inverted relative to the other conditions, the possible reasons for which have been discussed above. The EXAFS spectra reported here provide a volume-average coordination number, including the large particles on the surface. The actual metallic clusters in the Co−MCM-41 pore, therefore, may be smaller than the ones predicted here. This suggests the possibility of producing sub-nm Co clusters by proper treatments, and the size of clusters can be precisely controlled by combining the treatment methods and the pore size of the Co−MCM-41 samples, and their stabilities may be improved by anchoring to Co ions in the silica matrix.

To confirm the reliability of EXAFS for obtaining the metal cluster size by building a model, CO chemisorption was performed with a commercial instrument (Autosorb-1C, Quantachrome) for samples after TPR (where complete reduction has been achieved) as a complementary experiment. Each sample was pretreated at 673 K for 1 h under flowing ultrahigh purity hydrogen to reduce the Co clusters oxidized during exposure to the atmosphere, followed by vacuum treatment to clean the sample surface. Carbon monoxide adsorption was carried out at 313 K, and the stoichiometric ratio was assumed to be 1 (no CO dissociation). Table 4 shows the CO chemisorption results for each pore size of Co−MCM-41. The Co cluster sizes of samples show the same trend observed with the EXAFS results. The surface area and dispersion of Co clusters gradually increase as the pore size of Co−MCM-41 increases, resulting from different cluster sizes. When C10 and C16 Co−MCM-41 samples (as shown in TEM pictures) are compared, there are large differences in dispersion and surface area. This shows that, in the case of C10 Co−MCM-41, most of the Co clusters migrate out of the pores and form large particles on the surface. The Co−MCM-41 samples with larger pores still have high dispersion and surface area. This result supports the hypothesis

TABLE 4: CO Chemisorption Results of Co-MCM-41 Samples after TPR

samples	Co surface area (m^2/g)	Co dispersion (%)	average Co particle size (nm)
C10	0.6	9.3	10.8
C12	1.1	15.8	6.3
C14	1.4	20.8	4.8
C16	2.6	38.6	2.6
C18	5.0	74.5	1.3

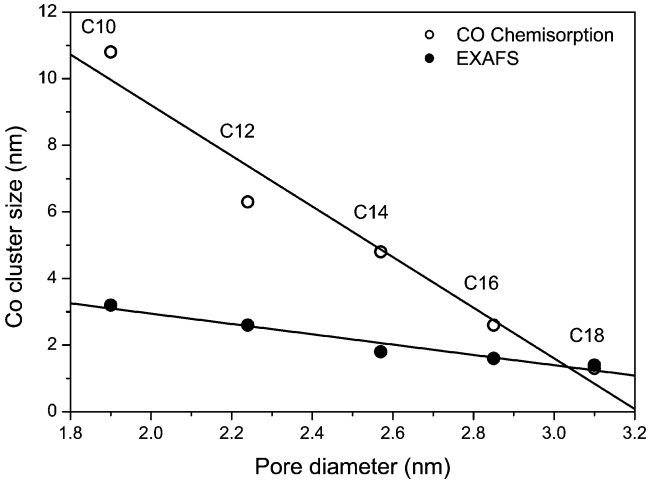

Figure 11. Co cluster sizes obtained by EXAFS and CO chemisorption with pore diameters.

that small pores produce bigger Co clusters after TPR by the higher migration rate and aggregation rate outside the pores. The Co cluster sizes obtained from EXAFS and CO chemisorption are compared in Figure 11. Both methods show linear correlations between the cluster and the pore sizes, but with different slopes. Co−MCM-41 with large pores show the similarity between two methods, but the differences in the cluster sizes grow as the pore size decreases, that is, Co clusters get larger. As mentioned earlier for particles smaller than 3−5 nm, by assuming a structural model, cluster sizes can be predicted from the coordination number obtained from the EXAFS experiment. The cluster size obtained from the average coordination number is sensitive to the shape. The average coordination number is most sensitive in the region below 2 nm, which is the region inaccessible or difficult to see by XRD or TEM. There is no lower size limit in EXAFS measurement;[53] indeed, the accuracy improves for very small metal clusters of a few atoms.[52] EXAFS and chemisorption should provide similar particle size measurement because both techniques have no limitation in the detection of the average cluster sizes of the surface metals. Chemisorption, however, may be a more accurate method for the measurement of large particles because of the size-sensitive limit of the coordination number obtained from EXAFS. In CO chemisorption results for completely reduced samples after TPR, only C16 and C18 Co−MCM-41 samples have cluster sizes in the coordination number sensitive range. The C14 Co−MCM-41 sample shows the limiting value of this range, and C12 and C10 samples have sizes beyond this range. This implies that the prediction of cluster sizes over 3−5 nm by EXAFS experiment is not reliable. The EXAFS experiment is also very insensitive to polydispersity of cluster sizes. The size can be underestimated when different sizes of clusters coexist on the surface.[54,55] However, all Co cluster sizes of samples treated by hydrogen reduction and CO disproportionation are under 1.5 nm so that the cluster sizes obtained earlier by EXAFS for these samples can be considered accurate values.

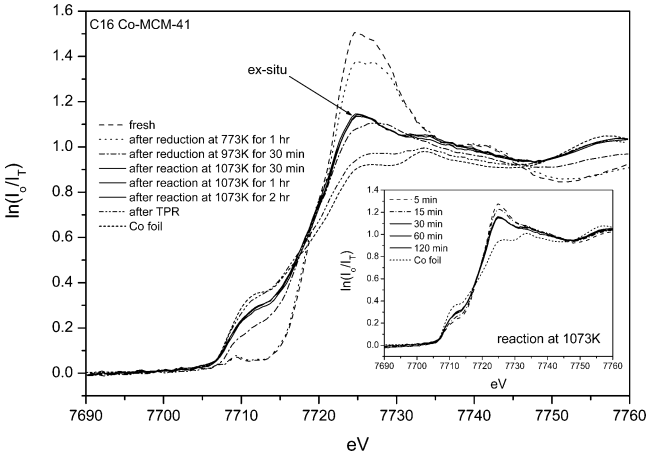

Figure 12. XANES spectra of C16 Co−MCM-41 treated in various ways. (inset: ex situ XANES spectra of C16 Co−MCM-41 samples after CO disproportionation for different reaction time).

Figure 12 shows XANES spectra of C16 Co−MCM-41 treated by the different methods mentioned so far. After reduction by hydrogen at 773 K for 1 h, only a decrease in the white line is noticed without any serious reduction of the Co atoms tetrahedrally coordinated with surrounding oxygen anions. When it is reduced at 973 K for 30 min, the formation of Co metal and a significant decrease of the white line are observed. Carbon monoxide disproportionation at 1073 K for different durations of time results in further growth of the Co metal peak with an increased white line due to the slight Co oxidation, resulting from ex situ measurement. The spectra of CO-reacted samples, however, are identical regardless of the reaction time. The inset figure shows XANES spectra taken for samples reacted with CO for different times. The Co metal peak grows as the reaction time increases and stops growing after 30 min. This may be attributed to the surface carbide produced with an onset of a certain size of the Co cluster, covering the clusters and protecting them from further growth. After TPR, the spectrum is almost identical to Co metal foil, which implies complete reduction of incorporated Co in MCM-41. These results suggest that CO disproportionation can be an effective method to control the Co cluster size by altering parameters such as prereduction temperature and time, reaction temperature, and CO concentration.

Conclusions

Very highly dispersed Co clusters may be synthesized by controlled reduction of cobalt ions isomorphously substituted for silicon ions in MCM-41. A major controlling factor is the radius of curvature of the pores in the Co−MCM-41 precursor, but several other parameters, such as the reducing agent, time, temperature, impurities, and structural order will also affect the reducibility of Co in Co−MCM-41. The total Co loading is also likely to affect both reducibility and final Co cluster size. However, for fixed Co loading, the synthesis conditions used in the preparation of the Co−MCM-41 appear to affect the distribution of the Co in the bulk of the pore wall or near surface, as does the radius of curvature of the pore wall. It appears that the Co distribution moves toward the interior of the wall as the radius of curvature decreases. Similar results are expected for other first-row transition metals, and thus metal−MCM-41 may provide a general method for obtaining highly dispersed and size controllable first-row transition metals in a MCM-41 matrix.

Acknowledgment. We are grateful to DoE-BES for the financial support of this project. Support by DARPA-DSO and the use of the National Synchrotron Light Source at Brookhaven National Laboratory is also gratefully acknowledged. Gary L. Haller wishes to dedicate this work to his good friend Michel Boudart. I was first introduced to Michel Boudart and his scholarship when he presented a seminar to Northwestern University graduate students almost exactly forty years ago. We now spend more time talking about art, led by Marina, but over those four decades, I have always been a student of Michel's on the subject of heterogeneous catalysis.

References and Notes

(1) Beck, J. S. US Patent 5, 057, 296, 1991.
(2) Beck, J. S.; Vartuli, J. C.; Roth, W. J.; Leonowicz, M. E.; Kresge, C. T.; Schmitt, K. D.; Chu, C. T. W.; Olson, D. H.; Sheppard, E. W.; McCullen, S. B.; Higgins, J. B.; Schlenker, J. L. *J. Am. Chem. Soc.* **1992**, *114*, 10834.
(3) Kresge, C. T.; Leonowicz, M. E.; Roth, W. J.; Vartuli, J. C. US Patent 5,102,643, 1992.
(4) Kresge, C. T.; Leonowicz, M. E.; Roth, W. J.; Vartuli, J. C. US Patent 5,098,684 1992.
(5) Beck, J. S.; Chu, C. T. W.; Johnson, I. D.; Kresge, C. T.; Leonowicz, M. E.; Roth, W. J.; Vartuli, J. C. US Patent 5,108,725, 1992.
(6) Kresge, C. T.; Leonowicz, M. E.; Roth, W. J.; Vartuli, J. C.; Beck, J. S. *Nature* **1992**, *359*, 710.
(7) Cheng, C. F.; Zhou, W. Z.; Park, D. H.; Klinowski, J.; Hargreaves, M.; Gladden, L. F. *J. Chem. Soc., Faraday Trans.* **1997**, *93*, 359.
(8) Corma, A.; Kan, Q. B.; Navarro, M. T.; PerezPariente, J.; Rey, F. *Chem. Mater.* **1997**, *9*, 2123.
(9) Sayari, A.; Kruk, M.; Jaroniec, M.; Moudrakovski, I. L. *Adv. Mater.* **1998**, *10*, 1376.
(10) Sayari, A.; Yang, Y.; Kruk, M.; Jaroniec, M. *J. Phys. Chem. B* **1999**, *103*, 3651.
(11) Matos, J. R.; Mercuri, L. P.; Kruk, M.; Jaroniec, M. *Chem. Mater.* **2001**, *13*, 1726.
(12) Guisnet, M.; Gnep, N. S.; Morin, S.; Patarin, J.; Loggia, F.; Solinas, V. *Mesoporous Molecular Sieves* **1998**, *117*, 591.
(13) Morin, S.; Ayrault, P.; ElMouahid, S.; Gnep, N. S.; Guisnet, M. *Appl. Catal., A* **1997**, *159*, 317.
(14) Constantin, C.; Parvulescu, V.; Bujor, A.; Popescu, G.; Su, B. L. *J. Mol. Catal., A* **2004**, *208*, 245.
(15) Parvulescu, V.; Constantin, C.; Popescu, G.; Su, B. L. *J. Mol. Catal., A* **2004**, *208*, 253.
(16) Yao, N. Ph.D. Thesis, Yale University, 2002.
(17) Joseph, T.; Hartmann, M.; Ernst, S.; Halligudi, S. B. *J. Mol. Catal., A* **2004**, *207*, 131.
(18) Lau, S. H.; Caps, V.; Yeung, K. W.; Wong, K. Y.; Tsang, S. C. *Microporous Mesoporous Mater.* **1999**, *32*, 279.
(19) Lim, S. Y.; Haller, G. L. *Appl. Catal., A* **1999**, *188*, 277.
(20) Mahalingam, R. J.; Badamali, S. K.; Selvam, P. *Chem. Lett.* **1999**, 1141.
(21) Krishna, R. M.; Kevan, L. *Phys. Chem. Chem. Phys.* **2001**, *3*, 5348.
(22) Balcar, H.; Sedlacek, J.; Cejka, J.; Vohlidal, J. *Macromol. Rapid Commun.* **2002**, *23*, 32.
(23) Paulino, I. S.; Schuchardt, U. *Catal. Commun.* **2004**, *5*, 5.
(24) Rahiala, H.; Beurroies, I.; Eklund, T.; Hakala, K.; Gougeon, R.; Trens, P.; Rosenholm, J. B. *J. Catal.* **1999**, *188*, 14.
(25) Spange, S.; Graeser, A.; Rehak, P.; Jager, C.; Schulz, M. *Macromol. Rapid Commun.* **2000**, *21*, 146.
(26) Ye, Z. B.; Zhu, S. P.; Wang, W. J.; Alsyouri, H.; Lin, Y. S. *J. Polym. Sci., Part B: Polym. Phys.* **2003**, *41*, 2433.
(27) Kallus, S.; Hahn, A.; Ramsay, J. D. F. *Eur. Phys. J. E* **2003**, *12*, S31.
(28) Kuchta, B.; Llewellyn, P.; Denoyel, R.; Firlej, L. *Low-Temperature Physics* **2003**, *29*, 880.
(29) Kumar, D.; Dey, G. K.; Gupta, N. M. *Phys. Chem. Chem. Phys.* **2003**, *5*, 5477.
(30) McNall, M.; Laurence, R. L.; Conner, W. C. *Microporous Mesoporous Mater.* **2001**, *44*, 709.
(31) Neimark, A. V.; Ravikovitch, P. I.; Grun, M.; Schuth, F.; Unger, K. K. *J. Colloid Interface Sci.* **1998**, *207*, 159.
(32) Ravikovitch, P. I.; Haller, G. L.; Neimark, A. V. *Adv. Colloid Interface Sci.* **1998**, *77*, 203.
(33) Ciuparu, D.; Chen, Y.; Lim, S.; Haller, G. L.; Pfefferle, L. *J. Phys. Chem. B* **2004**, *108*, 503.
(34) Lim, S.; Ciuparu, D.; Pak, C.; Dobek, F.; Chen, Y.; Harding, D.; Pfefferle, L.; Haller, G. *J. Phys. Chem. B* **2003**, *107*, 11048.
(35) Lim, S.; Haller, G. L. *Stud. Surf. Sci. and Catal.* **2000**, *130*, 3053.
(36) Lim, S.; Haller, G. L. *J. Phys. Chem. B* **2002**, *106*, 8437.
(37) Ciuparu, D.; Chen, Y.; Lim, S.; Haller, G. L.; Pfefferle, L. *J. Catal.*, in press.
(38) Jentys, A.; Pham, N. H.; Vinek, H.; Englisch, M.; Lercher, J. A. *Microporous Mater.* **1996**, *6*, 13.
(39) Jentys, A.; Pham, N. H.; Vinek, H.; Englisch, M.; Lercher, J. A. *Catal. Today* **1998**, *39*, 311.
(40) Khodakov, A. Y.; Griboval-Constant, A.; Bechara, R.; Villain, F. *J. Phys. Chem. B* **2001**, *105*, 9805.
(41) Khodakov, A. Y.; Griboval-Constant, A.; Bechara, R.; Zholobenko, V. L. *J. Catal.* **2002**, *206*, 230.
(42) Barrett, E. P.; Joyner, L. G.; Halenda, P. P. *J. Am. Chem. Soc.* **1951**, *73*, 373.
(43) Stern, E. A.; Newville, M.; Ravel, B.; Yacoby, Y.; Haskel, D. *Physica B* **1995**, *209*, 117.
(44) Feuston, B. P.; Higgins, J. B. *J. Phys. Chem.* **1994**, *98*, 4459.
(45) Galeener, F. L. *Solid State Commun.* **1982**, *44*, 1037.
(46) Clementi, E.; Raimondi, D. L. *J. Chem. Phys.* **1963**, *38*, 2686.
(47) Yang, Y.; Lim, S.; Wang, C.; Harding, D.; Haller, G. *Microporous Mesoporous Mater.* **2004**, *67*, 245.
(48) Wei, D.; Wang, H.; Feng, X. B.; Chueh, W. T.; Ravikovitch, P.; Lyubovsky, M.; Li, C.; Takeguchi, T.; Haller, G. L. *J. Phys. Chem. B* **1999**, *103*, 2113.
(49) Frenkel, A. I.; Hills, C. W.; Nuzzo, R. G. *J. Phys. Chem. B* **2001**, *105*, 12689.
(50) Tzou, M. S.; Teo, B. K.; Sachtler, W. M. H. *Langmuir* **1986**, *2*, 773.
(51) Tzou, M. S.; Jiang, H. J.; Sachtler, W. M. H. *Appl. Catal.* **1986**, *20*, 231.
(52) Via, G. H.; Sinfelt, J. H.; Lytle, F. W. *J. Chem. Phys.* **1979**, *71*, 690.
(53) Greegor, R. B.; Lytle, F. W. *J. Catal.* **1980**, *63*, 476.
(54) Moonen, J.; Slot, J.; Lefferts, L.; Bazin, D.; Dexpert, H. *Physica B* **1995**, *209*, 689.
(55) Bazin, D. C.; Sayers, D. A.; Rehr, J. J. *J. Phys. Chem. B* **1997**, *101*, 11040.